Nuclear Engineering and Technology 54 (2022) 4798–4808

Contents lists available at ScienceDirect

Nuclear Engineering and Technology

journal homepage: www.elsevier.com/locate/net

Original Article

Development of the vapor film thickness correlation in porous corrosion deposits on the cladding in PWR

Yuan Shen [a], Zhengang Duan [b], Chuan Lu [b], Li Ji [a], Caishan Jiao [a], Hongguo Hou [a], Nan Chao [a], Meng Zhang [a], Yu Zhou [a, **], Yang Gao [a, *]

[a] Fundamental Science on Nuclear Safety and Simulation Technology Laboratory, College of Nuclear Science and Technology, Harbin Engineering University, Harbin, 150001, Heilongjiang Province, China
[b] Science and Technology on Reactor System Design Technology Laboratory, Nuclear Power Institute of China, Chengdu, 610041, Sichuan Province, China

ARTICLE INFO

Article history:
Received 28 March 2022
Received in revised form
2 July 2022
Accepted 14 August 2022
Available online 20 August 2022

Keywords:
Vapor film thickness
CRUD
Multi-physics
Heat transfer model
Fuel rods

ABSTRACT

The porous corrosion deposits (known as CRUD) adhered to the cladding have an important effect on the heat transfer from fuel rods to coolant in PWRs. The vapor film is the main constituent in the two-phase film boiling model. This paper presents a vapor film thickness correlation, associated with CRUD porosity, CRUD chimney density, CRUD particle size, CRUD thickness and heat flux. The dependences of the vapor film thickness on the various influential factors can be intuitively reflected from this vapor film thickness correlation. The temperature, pressure, and boric acid concentration distributions in CRUD can be well predicted using the two-phase film boiling model coupled with the vapor film thickness correlation. It suggests that the vapor thickness correlation can estimate the vapor film thickness more conveniently than the previously reported vapor thickness calculation methods.

1. Introduction

The corrosion of structural materials is a challenging issue for the aim of reactor life extension. Even though structural materials in reactors are corrosion-resistant, the contact area of the structural materials to the coolant is up to 25000 m^2, and can lead to a large number of corrosion products releasing into the primary coolant [1,2]. Part of the corrosion products can deposit onto fuel cladding, and the deposits is called CRUD. CRUD can impose some influences on the safe and stable operation of reactors, including (1) CRUD induced power shift (CIPS), which results from the concentrated boron due to the sub-cooled nucleate boiling in CRUD [3]; (2) CRUD induced localized corrosion (CILC), which is caused by the increase of thermal resistance [4]; (3) CRUD induced irradiation field formation, which brings a higher occupational exposure during maintenance and reactor shutdown. The first two phenomena are closely related to the heat transfer characteristic of CRUD, therefore, modeling the heat transfer in CRUD has been the focus of attention.

Until now, various heat transfer models have been developed. In 1974, Cohen developed a 1D heat transfer model for the porous deposit and it was assumed that liquid was drawn into CRUD from small pores and vapor was ejected from large pores [5]. Subsequently, Pan et al. [6] proposed a 2D wick boiling model and predicted the maximum concentration factor in CRUD. Henshaw et al. [7] coupled the various chemical reactions into the heat transfer model, including the radiolysis of water, boric acid chemistry, the precipitation of $LiBO_2$. Haq et al. [8] further improved the two-dimensional coupled wick boiling model and discussed the differences of the heat transfer performance by coupled and uncoupled models. Short et al. [9] introduced fractal geometric parameters into the 2D model to calculate the CRUD thermal conductivity and permeability more precisely. Park et al. [10] fully coupled multi-physics behaviors including heat transfer, fluid dynamics, mass transport, chemical reactions, radiolysis, and surface reactions into the heat transfer model.

The models mentioned above are mostly based on wick boiling, in which porous solid medium was assumed to be full of liquid. However, at the case of a high heat flux in PWR (the core average is 0.5 MW/m^2, the hottest-rod average is 1 MW/m^2, and the local peak heat flux is 1.5 MW/m^2), the predicted CRUD effective thermal conductivity was higher than the experimental values, along with

* Corresponding author.
** Corresponding author.
E-mail addresses: ervin@hrbeu.edu.cn (Y. Zhou), gaoyang@hrbeu.edu.cn (Y. Gao).

https://doi.org/10.1016/j.net.2022.08.013

unrealistically high predicted liquid superheat [9]. Therefore, other heat transfer mechanisms were introduced into CRUD heat transfer models together with wick boiling, especially film boiling. Wang et al. [11] studied the CRUD thermal conductivity for different CRUD-regimes at PWR operating conditions by experiments and the results can be used to validate the various heat transfer models including the film boiling model. Jin et al. [12] proposed a two-phase film boiling model, in which the vapor thickness was initially set as a certain value and then corrected. Collier et al. [8,13] proposed a derived equation using the Clausius-Clapeyron relation to calculate the vapor film thickness, in which a few CRUD properties were considered but no solute was assumed in the liquid. However, it is a fact that the solute has a large concentration factor due to the boiling regime, which affects both the surface tension and the saturation temperature [8]. Recently, Yeo et al. [14] developed a method to calculate the vapor film thickness from the perspective of hydrodynamic balance at the interface between the vapor film and liquid region, which analyzed more physical mechanisms to explain the formation of the vapor film than their previous empirical formulation describing the heat-flux dependent behavior of the driving force [14]. This calculation method can give an accurate vapor film thickness by coupling with a film boiling model. It is a fact that the vapor film thickness depends strongly on the CRUD properties and operational conditions. However, it cannot intuitively obtain the relationship between the vapor film thickness and various factors according to this method. Additionally, a large number of iterative computations was required during the prediction of heat transfer in CRUD due to the coupling with the film boiling model according to our study. Therefore, it is necessary to develop an intuitive vapor film thickness correlation, in which the effects of the CRUD properties and operational conditions on vapor film thickness can be directly revealed.

In this paper, a vapor film thickness correlation is proposed based on multivariate regression analysis after the sensitivity analysis of the effects of various factors, such as CRUD chimney density, CRUD porosity, CRUD particle size, CRUD thickness, CRUD pore size and heat flux on the film thickness. This correlation can intuitively reflect the effects of CRUD properties and operational conditions on the vapor thickness. This model is then introduced into a two-phase film boiling model to predict the heat transfer characteristics of CRUD and the results are demonstrated to be reliable.

2. Modeling description and solution

2.1. Physical processes in CRUD

CRUD is the porous media within a number of the chimneys. It adheres to the surface of the cladding and influences the heat transfer between the cladding surface and coolant. The heat transfer regime within CRUD in the present study is considered to have an extra vapor-saturated region (the vapor film) than the typical wick boiling model. The details of the CRUD structure and the physical processes are shown schematically in Fig. 1. The heat removal from the cladding to coolant depends on three processes, including the conduction in CRUD, the evaporation on the chimney wall or on the boundary of the vapor film and the liquid film, and the convective heat transfer between the coolant and CRUD. The evaporation of liquid within CRUD leads the coolant permeate into the porous media, while the bubbles produced by the evaporation can flow back into the bulk coolant through the steam chimney.

2.2. Estimation of vapor film thickness

Eq. (1) is the relation to estimate the vapor film thickness (δ_v)

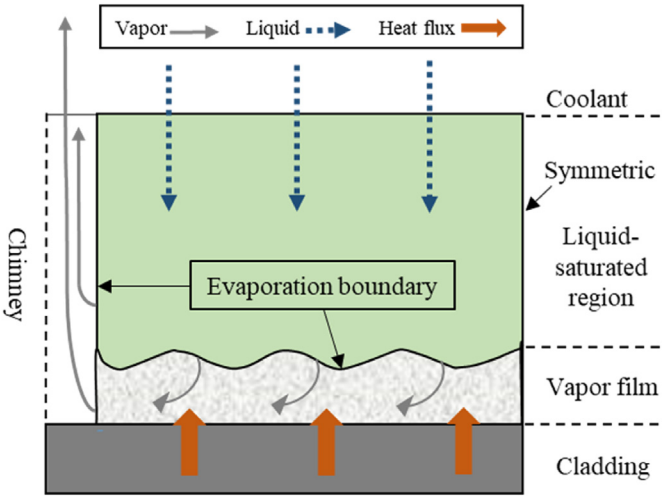

Fig. 1. The schematic of CRUD and the physical processes.

which was derived from the hydrodynamic balance equation proposed by Yeo et al. [14]. It was assumed that the pressure from vapor is equal to the pressure from liquid plus capillary force or disjoining force on the menisci in pores near the interface. For the case where capillary force is dominant, the vapor film thickness δ_c* is smaller than δ_d* for disjoining force case, because the growth of the vapor film is suppressed more largely by the capillary force. Similarly, for the case where disjoining force is dominant, δ_d* is smaller than δc* [14]. As a result, the vapor film thickness is equal to the minimum film thickness between the two.

$$\delta_v = \delta \times \min(\delta_c^*, \delta_d^*) \tag{1}$$

where δ is the CRUD thickness, and δ_c^* is the vapor film thickness for the capillary dominant case expressed in Eq. (2).

$$\delta_c^* = \frac{1}{2}\left[\sqrt{\left(2\frac{r^* cos\phi}{1+\beta f^*}\frac{Da}{Ca}-1\right)^2+\frac{2\beta d^{*2}}{1+\beta f^*}}-\left(2\frac{r^* cos\phi}{1+\beta f^*}\frac{Da}{Ca}-1\right)\right] \tag{2}$$

where the parametric expressions are $r^* = \frac{\lambda}{\delta}$, $Da = \frac{\kappa}{\lambda^2}$, $\beta = \frac{\upsilon_v}{\upsilon_l}$, $f^* = \frac{32\kappa(1-f_{ch})}{f_{ch}d_{ch}^2}$, $Ca = \frac{\upsilon_l q}{\sigma_{lv}h_{fg}(1-f_{ch})}$, $d^* = \frac{d_{esc}}{\delta}$, $f_{ch} = n_{ch}\frac{\pi d_{ch}^2}{4}$, $d_{esc} = \frac{1}{\sqrt{2n_{ch}}}$. Concerning the CRUD properties, it involves average pore size λ, CRUD thickness δ, chimney density n_{ch}, porosity (reflected in permeability κ) and chimney diameter d_{ch}. The other parameters include contact angle ϕ, vapor kinematic viscosity υ_v, liquid kinematic viscosity υ_l, heat flux q, the enthalpy of vaporization of the fluid h_{fg}.

2.3. Two-phase film boiling model

2.3.1. Liquid-saturated CRUD region modeling

(1) Heat transfer modeling

The governing equation (3) for the temperature field in the liquid-saturated CRUD region contains conduction term and convection term.

$$-\nabla.(k_{sl}\nabla T_l) + \rho c_p \tau\left(\frac{K}{\mu\varepsilon}\nabla P_l\right)\nabla T_l = 0 \tag{3}$$

Where T_l is the temperature in Liquid-saturated CRUD region, ρ is the fluid density, c_p is the specific heat capacity of the fluid, μ is the fluid viscosity, and P_l is the pressure. k_{sl} denotes the thermal conductivity of the liquid region.

The boundary conditions are listed as follows:

$$-k_{sl}\frac{\partial T_l}{\partial n}=h_c(T_l-T_{coolant});\ \text{at}\ \Gamma\ =\ \Gamma_{\text{coolant}}$$

$$\frac{\partial T_l}{\partial n}=0;\ \text{at}\ \Gamma=\ \Gamma_{\text{symmetric}}$$

$$T_l=T_{sat};\ \text{at}\ \Gamma=\Gamma_{\text{interface}}$$

$$T_l=T_{sat};\ \text{at}\ \Gamma=\Gamma_{\text{chimney}}$$

where Γ with four different subscripts denotes the four specific boundaries in the CRUD unit, n is a vector normal to a boundary, h_c is the coolant convection heat transfer coefficient, and $T_{coolant}$ is the bulk coolant temperature.

(2) Coolant flow modeling

Fluid flow in CRUD follows Darcy's law and the effect of gravity is negligible due to the much larger pressure difference driven by the capillary force in CRUD. In Darcy's law, the velocity of the fluid in the porous media is proportional to the pressure gradient as follows:

$$-\nabla\left(\frac{\kappa}{\mu\varepsilon}\nabla P_l\right)=0 \tag{4}$$

the true fluid velocity $\boldsymbol{v}$ is defined as follows:

$$v=-\frac{\kappa}{\mu\varepsilon}\nabla P_l \tag{5}$$

The boundary conditions are listed as follows:

$$P_l=P_{coolant};\ \text{at}\ \Gamma=\Gamma_{\text{coolant}}$$

$$\frac{\partial P_l}{\partial n}=0,\ \text{at}\ \Gamma=\ \Gamma_{\text{symmetric}}$$

$$\frac{\kappa}{\mu}\frac{\partial P_l}{\partial n}=\frac{1}{\rho h_{fg}}\cdot\left(-k_{sl}\frac{\partial T_l}{\partial n}+k_{sv}\frac{\partial T_v}{\partial n}\right),\ \text{at}\ \Gamma=\Gamma_{\text{interface}}$$

$$\frac{\kappa}{\mu}\frac{\partial P_l}{\partial n}=\frac{-k_{sl}}{\rho h_{fg}}\cdot\frac{\partial T_l}{\partial n},\ \text{at}\ \Gamma=\Gamma_{\text{chimney}}$$

Where $P_{coolant}$ is the pressure of the primary coolant system, and T_v is the temperature distribution in the vapor-saturated CRUD region.

(3) Solute transport modeling

The coolant solute transports into the CRUD, and it can also affect the saturation temperature and the vapor formation in the porous medium. The boric acid is the only one considered species to be coupled in the model since it is one of the most important species in coolant to affect the saturation temperature [15]. The governing equation of boric acid transport is expressed as follows:

$$-D\nabla^2C+v\nabla C=0 \tag{6}$$

where D is the boric acid diffusion coefficient in water and C is the boric acid concentration distribution in liquid-saturated CRUD region in this study.

The boundary conditions are listed as follows:

$$C=C_{bulk};\ \text{at}\ \Gamma=\Gamma_{\text{coolant}}$$

$$D\frac{\partial C}{\partial n}=0;\ \text{at}\ \Gamma\ =\Gamma_{\text{symmetric}}$$

$$-D\frac{\partial C}{\partial n}+\boldsymbol{v}.\boldsymbol{n}C=0;\ \text{at}\ \Gamma=\Gamma_{\text{interface}}$$

$$-D\frac{\partial C}{\partial n}+\boldsymbol{v}.\boldsymbol{n}C=0;\ \text{at}\ \Gamma=\Gamma_{\text{chimney}}$$

where the concentration of boric acid in the bulk coolant C_{bulk} is set to 80 mol/m^3.

2.3.2. Vapor-saturated CRUD region modeling

The differential equations for the temperature and velocity fields are similarly considered to those used in the liquid-saturated CRUD region but solved for the different boundary conditions, and vapor-based properties replace water-based liquid properties. Solute transport is neglected in this region.

(1) heat transfer modeling

For the temperature field, the boundary conditions are listed as follows:

$$T_v=T_{sat};\ \text{at}\ \Gamma=\Gamma_{\text{interface}}$$

$$\frac{\partial T_v}{\partial n}=0:\ \text{at}\ \Gamma=\Gamma_{\text{symmetric}}$$

$$-k_{sv}\frac{\partial T_v}{\partial n}=q;\ \text{at}\ \Gamma=\Gamma_{\text{clad}}$$

$$-k_{sv}\frac{\partial T_v}{\partial n}=-\rho h_g\frac{\kappa}{\mu}\frac{\partial P_v}{\partial n};\ \text{at}\ \Gamma=\Gamma_{\text{chimney}}$$

where h_g is the superheated vapor enthalpy.

(2) Coolant flow modeling

For the velocity field, the boundary conditions are listed as follows:

$$P_v=P_l+P_{capillary};\ \text{at}\ \Gamma=\Gamma_{\text{interface}}$$

$$\frac{\partial P_v}{\partial n}=0;\ \text{at}\ \Gamma=\Gamma_{\text{symmetric}}$$

$$\frac{\partial P_v}{\partial n}=0;\ \text{at}\ \Gamma=\Gamma_{\text{clad}}$$

$$\int_{chimney}\left(\rho\left(-\frac{\kappa}{\mu\varepsilon}\frac{\partial P}{\partial n}\right)\right)_v ds=\int_{interface}\left(\rho\left(-\frac{\kappa}{\mu\varepsilon}\frac{\partial P}{\partial n}\right)\right)_l ds:$$
$$\text{at}\ \Gamma\ =\Gamma_{\text{chimney}}$$

where P_v is the pressure distribution in the Vapor-saturated CRUD region. It was indicated that in the case of a thin vapor film, the capillary force is dominant, and the disjointing force can be

omitted. The disjointing force need to be considered in the case of the CRUD nearly occupied by the vapor film [12,14]. In our study, CRUD is partial dry-out and vapor film thickness is not very large. Therefore, only the capillary pressure is added to the liquid pressure, which is also reflected in Eq. (1), the vapor film thickness δ_c^* for the capillary dominant case is mainly considered. The capillary pressure is calculated by Eq. (7)

$$P_{capillary} = \frac{2\sigma(T)\cos\theta}{\lambda} \tag{7}$$

where the contact angle θ is assumed to 0, and σ is the surface tension of water calculated by Eq. (8).

$$\sigma = B\left[\frac{T_c - T}{T_c}\right]^{1.256}\left[1 + b\left(\frac{T_c - T}{T_c}\right)\right] \tag{8}$$

where $B = 235.8 \times 10^{-3}$N/m, $b = -0.625$, $T_c = 647.15$K.

2.3.3. Parametric equations in the model

(1) Saturation temperature

The saturation temperature of water with high amounts of boric acid expressed by Eq. (9) is from Deshon [16]. A polynomial function was fit to the data, with boric acid concentrations scaled to mole fractions in the fluid inside the CRUD.

$$T_{sat} = 618.09 + 199.01(1-a_w) - 952.74(1-a_w)^2 + 26013.9(1-a_w)^3 - 262916.0(1-a_w)^4 + 997166.1(1-a_w)^5$$

where a_w is the activity of water, defined as follows:

$$a_w = \frac{m_w}{m_w + \sum_{all} m_i} \tag{10}$$

where m_w is molar concentration of water and m_i is molar concentration of boric acid in this study.

(2) CRUD thermal conductivity

The calculation of CRUD thermal conductivity includes the CRUD thermal conductivity of the vapor-saturated region and the CRUD thermal conductivity of the liquid-saturated region. Eqs. (11)–(13) are used to estimate the thermal conductivity of the vapor-saturated CRUD (k_{sv}) based on the parallel and series layer models [9], which are widely used to predict the thermal conductivity of a two-phase system [17]:

$$k_{sv} = \frac{2}{k_{parallel}^{-1} + k_{series}^{-1}} \tag{11}$$

$$k_{parallel} = \frac{\left(2 - D_f\right)\varepsilon\lambda_{max}^{D_T-1}\left[1 - \left(\frac{\lambda_{min}}{\lambda_{max}}\right)^{D_T - D_f + 1}\right]}{L^{D_T-1}\left(D_T - D_f + 1\right)\left[1 - \left(\frac{\lambda_{min}}{\lambda_{max}}\right)^{2-D_f}\right]}k_v + (1-\varepsilon)k_s \tag{12}$$

$$k_{series} = \frac{1}{\frac{\varepsilon}{k_v} + \frac{1-\varepsilon}{k_s}} \tag{13}$$

where ε is the porosity, L is a characteristic length of the system, D_f is the pore free area dimension, and D_T is the tortuous capillarity dimension [9] as follows:

$$D_f = d_e - \frac{\ln(\varepsilon)}{\ln\left(\frac{\lambda_{min}}{\lambda_{max}}\right)} \tag{14}$$

$$D_T = 1 + \frac{\ln(\tau)}{\ln\left(\frac{L}{\lambda_{min}}\right)} \tag{15}$$

$$L = \lambda_{max}\sqrt{\frac{\pi}{4}\frac{D_f}{2 - D_f}\frac{(1-\varepsilon))}{\varepsilon}} \tag{16}$$

where d_e is the simulating dimension (d_e is set to 2 for the present 2-D model). The minimum pore size $\lambda_{\min}$ is assumed to be 0.25 μm, which is the same as the previous value [10,12,18]. The maximum pore size λ_{max} is in the range of 0.4–0.8 μm and is set differently by case. The maximum pore size is set to be 0.5 μm when the other parameters vary. When the effect of the maximum pore size on the vapor film thickness is studied, the maximum pore size is in the range of 0.4–0.8 μm and is set to be 0.4, 0.5 μm and so on.

The thermal conductivity of the solid part of the CRUD (k_s) is assumed to be 4.5 W/(m K) [19], and the thermal conductivity of vapor (k_v) is taken from Ref. [20] as follows:

$$k_v = -7.21\times10^{-3} + P\left(8.309\times10^{-8} + 2.818\times10^{-15}P\right) + T\left(6.74\times10^{-5} + 3.895\times10^{-8}T\right) + TP\left(-2.854\times10^{-10} - 4.067\times10^{-18}P + 2.417\times10^{-13}T\right) \tag{17}$$

where P is the pressure in Pa and T is the temperature in degrees Kelvin.

The thermal conductivity of the liquid-saturated CRUD (k_{sl}) is set to 0.706 W/(m K) for the CRUD with the porosity within the range from 0.40 to 0.70, which is an average value of the two case ends of the porosity range calculated by a generally used model expressed as Eqs.(18)–(20) [7]. The thermal conductivity of the liquid-saturated CRUD with the porosity of 0.40 is calculated for 0.5996 W/(m K) at 610 K (the temperature is the average value of coolant temperature 600K and the saturated temperature about 619 K with the boric concentration in bulk coolant) and with the porosity of 0.70 is calculated for 0.8121 W/(m K) at 610 K.

$$k_{sl} = k_w\frac{1 - (1 - bk_s)(1-\varepsilon)}{1 + (b-1)(1-\varepsilon)} \tag{18}$$

$$b = \frac{3k_w}{2k_w + 2k_s} \tag{19}$$

$$k_w = 0.616 + 9.46\times10^{-4}T - 2.82\times10^{-6}T^2 - 3.61\times10^{-9}T^3 \tag{20}$$

(3) Permeability

The flow permeability is calculated by the Kozeny-Carmen equation as expressed in Eq. (21), which has been used for CRUD and the results have been suggested to be consistent with those by the in-core or autoclave experiments [8,10]. Compared to the fractal permeability formula in Ref. [14], the form of Eq. (21) is more simplified.

$$\kappa = \frac{\varepsilon^3 d_p^2}{150(1-\varepsilon)^2} \tag{21}$$

where d_P is the particle size of CRUD, which was assumed to 0.25 μm in the previous report [10], while the particle size of 0.20–0.40 μm in CRUD is considered in this study.

(4) Coolant properties

Eqs. (22)–(24) are used to calculate the water density, the specific heat capacity of the water, the water viscosity, respectively.

$$\rho_l = 997 + 2.01\times10^{-1}T(℃) - 8.16\times10^{-3}T(℃)^2 + 2.91\times10^{-5}T(℃)^3 - 4.44\times10^{-8}T(℃)^4 \tag{22}$$

$$c_p = 4028 + \frac{128.8}{(1-\frac{T}{650})} + \frac{4.674}{\left(1-\frac{T}{650}\right)^2} \tag{23}$$

$$\mu_l = \frac{25.3}{-85800 + 91T + T^2} \tag{24}$$

Eqs. (25)–(27) are used to calculate the vapor density, the specific heat capacity of the vapor, the vapor viscosity, respectively.

$$\rho_v = 0.576 + P\left(2.483\times10^{-5} - 1.410\times10^{-12}P\right) + \frac{P}{T}\left(-2.616\times10^{-2} + 1.016\times10^{-9}P\right) + \frac{7.589}{T} \tag{25}$$

$$c_{p,v} = 2709 + \frac{P}{T}\left(-8.594\times10^{-1} - 2.378\times10^{-7}P + 1.062\times10^{-3}T + 1.686\times10^{-4}\frac{P}{T}\right) - 277.2\frac{T^2}{P} \tag{26}$$

$$\mu_v = \frac{11.4}{1.37\times10^6 - 844T - T^2} \tag{27}$$

2.4. Coupling scheme and solution

The above analyzed physical processes of the film boiling model including heat transfer, coolant flow, solute transport in the liquid-saturated and vapor saturated regions are fully coupled. For the liquid-saturated CRUD region, the heat transfer model calculates the temperature distribution using saturation temperature which is obtained from the solute transport model, and provides evaporative coolant flux to the coolant flow model. The coolant flow model calculates the pressure distribution using the chimney coolant mass flux and provides convective mass flux to the solute transport model. The solute transport equation is solved to derive the species concentration at the chimney wall, then the saturation temperature boundary condition can be modified. For the vapor-saturated CRUD region, the coupling scheme is almost the same but without a solute transport equation. The liquid-saturated and vapor-saturated regions are connected by joint boundary conditions.

Due to the introduction of the vapor film thickness into the film boiling model, the coupling of the vapor film thickness and the film boiling model need to be realized besides the coupling of the different physical processes considered in the film boiling model. Therefore, the calculations are correspondingly divided into two parts: one is realized by COMSOL Multiphysics to deal with the coupling analyzed above and calculate the liquid temperature, liquid pressure, dissolved species concentration, vapor temperature, and vapor pressure in CRUD; the other is realized by a self-compiled program to deal with the coupling between the vapor film thickness and the film boiling model.

Fig. 2 presents the process of the coupling between the film boiling model and the vapor film thickness. The green rectangular in Fig. 2 represents the film boiling model calculated by COMSOL, and the blue rectangular in Fig. 2 shows the dealing of the coupling between the vapor film thickness and the film boiling model realized by the self-compiled program. An initial saturation temperature T_{sat} is set to calculate the corresponding vapor film thickness. Then the boundary temperature $T_{interface}$ between the vapor-saturated region and liquid-saturated region can be obtained by the COMSOL Multiphysics. The above processes are repeated until the difference between T_{sat} and $T_{interface}$ is less than 0.5. When the whole calculation is accomplished, the distributions of temperature, pressure and boric acid concentration within the two regions can be exported from COMSOL Multiphysics as well as the vapor film thickness and the effective thermal conductivity in CRUD.

3. Results and discussion

3.1. Validation

The temperature, pressure, and boric acid concentration in CRUD are calculated using the two-phase film boiling model combined with the vapor film thickness method described in **section 2.1**. The calculated CRUD/Clad mean temperature is compared with the results reported by the WALT loop test [21] and Jin's report [12], as shown in Fig. 3, and the input values of the parameters are mainly taken from Jin's report [12]. It is found that the relative errors between our model and the WALT test were generally smaller than those between Jin's model and the WALT test with the same input simulated parameters. It suggests that the film boiling model coupled with the vapor film thickness equation (described in section 2.2) can obtain a more realistic peak temperature in CRUD than that of the previous study [12]. The vapor film thicknesses are 0.66–5.7 μm here, and 7~8 μm in Jin's model [12].

The effective thermal conductivity of the five rod cases is calculated and compared with those obtained by the film boiling model [12], as presented in Table 1. It can be seen that the results

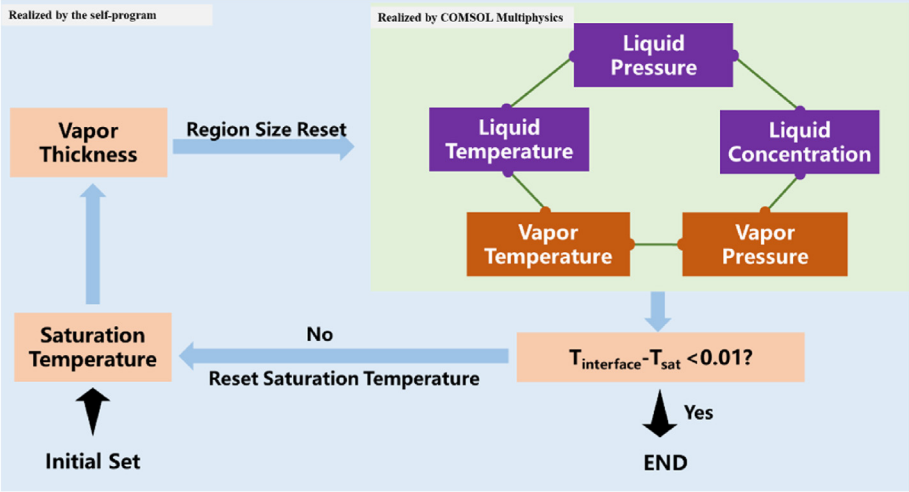

Fig. 2. The solution flow chart of the model.

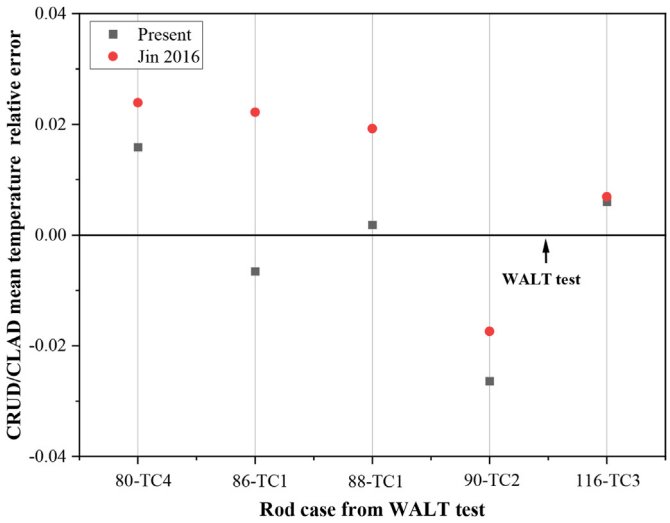

Fig. 3. Relative errors from the comparison of the CRUD/CLAD temperature between models and the WALT loop experiment result.

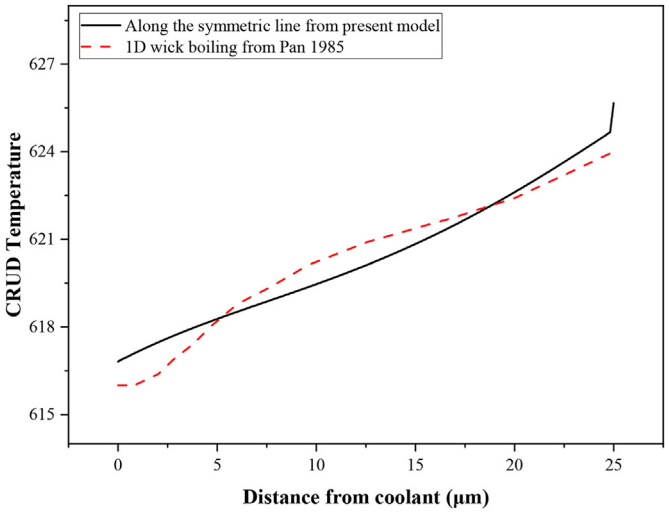

Fig. 4. CRUD temperature distribution calculated by the present model and the wick boiling model, the latter was performed by Pan et al. [6].

are close to those reported by Jin [12] in general, and the maximum difference between the effective thermal conductivity is 0.39 W/m K, which is attributed to the different calculated vapor film thickness. The vapor film thicknesses are 0.66–5.7 μm here, and 7~8 μm in Jin's model [12]. In addition, the other experimental effective thermal conductivity was in the range of 0.82–1.12 W/m K with the porosity of 0.46–0.6 [21,22], and the simulated results are obviously within this scope.

The temperature distribution in CRUD calculated by our model and the wick boiling model is shown in Fig. 4. The two curves approach each other, but there exists a sharp increase in the temperature in the vicinity of the cladding in our results. In our study, a vapor film region in CRUD was assumed, while only wick boiling regime was considered in Ref. [6]. Therefore, the change trend of temperature in the CRUD adjacent to cladding is different. The sharp increase of temperature at CRUD-to-cladding interface was also reported by Yeo [14]. It implies that the heat removal decreases due to the existence of vapor film, so the temperature elevates dramatically, which will accelerate the cladding corrosion [23].

3.2. Sensitivity analysis of CRUD properties and heat flux

The effects of CRUD porosity, CRUD pore size, CRUD particle size, CRUD chimney density, CRUD thickness on the CRUD/CLAD

Table 1
Comparison of the calculated effective thermal conductivity.

Model	Calculated effective thermal conductivity (W/m K)				
	Rod80-TC4	Rod86-TC1	Rod88-TC1	Rod-90-TC2	Rod116-TC4
Present model	0.80	1.18	1.05	0.74	0.61
Jin 2016 [12]	1.01	0.84	1.07	1.08	1.00

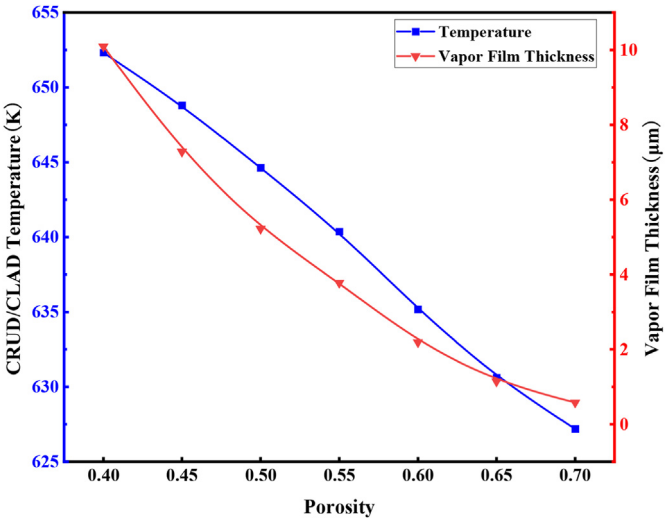

Fig. 5. Effect of CRUD porosity on CRUD/CLAD temperature and vapor film thickness.

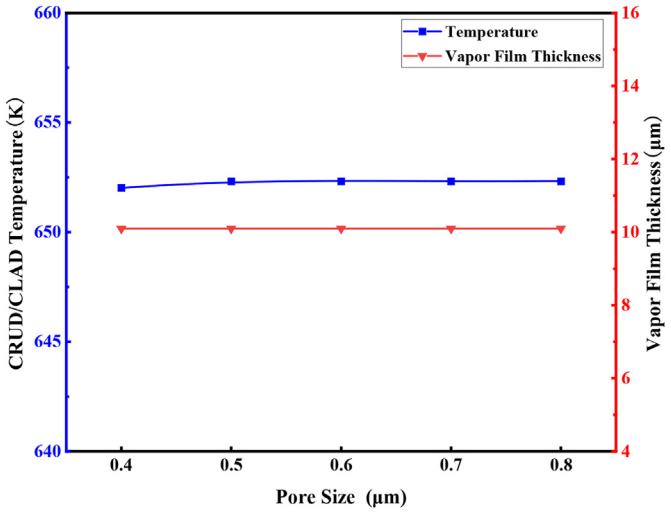

Fig. 6. Effect of CRUD pore size on CRUD/CLAD temperature and vapor film thickness.

temperature and the vapor film thickness are shown in Fig. 5 to Fig. 9. Both the cladding surface mean temperature and the vapor film thickness decrease with the increase of the CRUD porosity, which is attributed to more liquid in the CRUD with a larger porosity [12]. According to the typical heat capacity formula (28), the heat absorbed by the liquid per unit time is related to the mass and the specific heat capacity of the liquid.

$$\Delta Q = mC\Delta T \tag{28}$$

When the heat flux is assumed to be equal in CRUD with different porosities, the heat capacity formula (28) can be transferred to Eq. (29) as follows:

$$m_1 C(T_1 - T_{sat}) - m_2 C(T_2 - T_{sat}) = 0 \tag{29}$$

where m is the liquid mass, C is the liquid heat capacity, and T is the mean CRUD temperature, subscript *1* denotes the CRUD with a larger porosity and subscript *2* is the CRUD with a smaller porosity. CRUD with a larger porosity can hold more liquid which means to expand the wick boiling region and then thin the vapor film thickness. Therefore, T_1 corresponding to the CRUD with a larger wick boiling region is lower than T_2 that within a smaller wick boiling region, which results in the decrease of the CRUD/CLAD temperature with the increase of the CRUD porosity. The vapor film thickness positively correlated with the temperature, so it decreases with the increase of the porosity in Fig. 5. In addition, the larger the porosity, the larger liquid mass in CRUD, then the larger the heat capacity. Therefore, the increase of temperature in CRUD is smaller in the case of large porosity than that in the case of small porosity at the same heat flux and reduce the production of the vapor.

The effect of the pore size on the CRUD/CLAD temperature and vapor film thickness is plotted in Fig. 6. According to the relation of CRUD pore size and porosity, the temperature and thickness seem to decrease with the increase of the CRUD pore size. However, both the CRUD/CLAD temperature and the vapor film thickness are weakly dependent on the CRUD pore size, which is consistent with the results from Ref. [12]. Here, the CRUD porosity ε is assumed to be equal to the ratio of the pore volume V_{pore} to the solid shell volume V_{shell} as shown in Eq. (30). The number of pores in CRUD with different porosities is assumed to be a fixed value.

$$\varepsilon = \frac{V_{pore}}{V_{shell}} = \frac{n\left(\frac{4}{3}\pi {r_{po}}^3\right)}{\left(1 - n_{ch}\pi r_{ch}^2\right)\delta} \tag{30}$$

where n is the pore number in mm^{-2}, r_{po} is the pore radius in mm, and r_{ch} is the chimney radius in mm. Typically, $\varepsilon = 0.8$, $r_{po} = 2 \times 10^{-4}$ mm, $n_{ch} = 2 \times 10^3 mm^{-2}$, $r_{ch} = 2.5 \times 10^{-3}$ mm, $\delta = 2.5 \times 10^{-2}$mm, and the calculated n is nearly 5×10^8 mm^{-2}, thus the CRUD porosity can be expressed as:

$$\varepsilon = 8.7 \times 10^{10} r^3 \tag{31}$$

According to Eq. (31), the CRUD porosity changes little with the pore size in the studied range of 0.4–0.8 μm. Therefore, the CRUD/CLAD temperature and the vapor film thickness only fluctuate slightly with the pore size as shown in Fig. 6. The dependence of the CRUD/CLAD temperature and the vapor thickness on the chimney density is illustrated in Fig. 7. With the increase of the CRUD chimney density, the temperature and the thickness decrease,

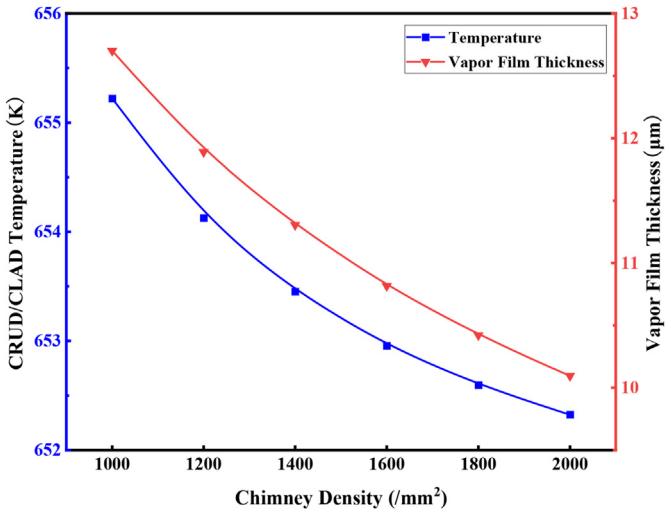

Fig. 7. Effect of CRUD chimney density on CRUD/CLAD temperature and vapor film thickness.

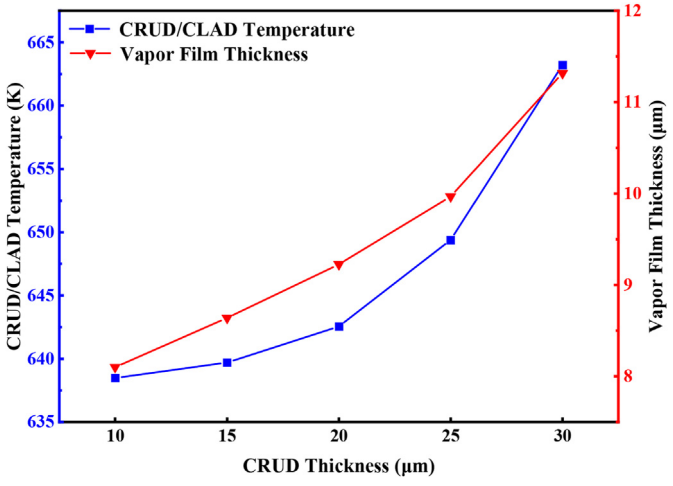

Fig. 8. Effect of CRUD thickness on CRUD/CLAD CRUD/CLAD temperature and vapor film thickness.

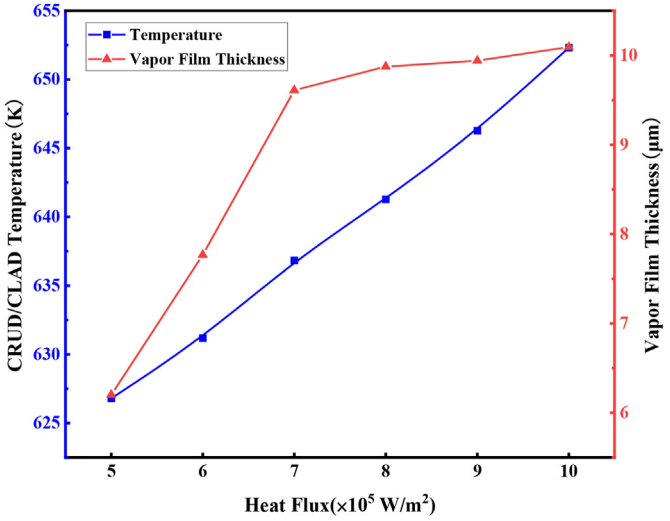

Fig. 10. Effect of heat flux on CRUD/CLAD temperature and vapor film thickness.

which is consistent with Yeo's results [18]. The increase of the chimney number means the expanding of the boiling heat removal area, so the CRUD/CLAD temperature decreases while the vapor thickness also decreases.

The impact of the CRUD thickness on the CRUD/CLAD temperature and the vapor thickness is shown in Fig. 8. With the increase of the CRUD thickness, the temperature and the vapor film thickness increase. The increase of the CRUD thickness causes the increase of the thermal resistance, and the flow route of both the liquid phase and the vapor phase becomes longer and the flow resistance strengthens. As a result, the CRUD/CLAD temperature and vapor film thickness increase.

The effect of CRUD particle size on CRUD/CLAD temperature and vapor film thickness is shown in Fig. 9. With the increase of the particle size, the temperature and the thickness decrease. Since the flow permeability increases with the increase of the particle size, more liquid penetrates into the CRUD.

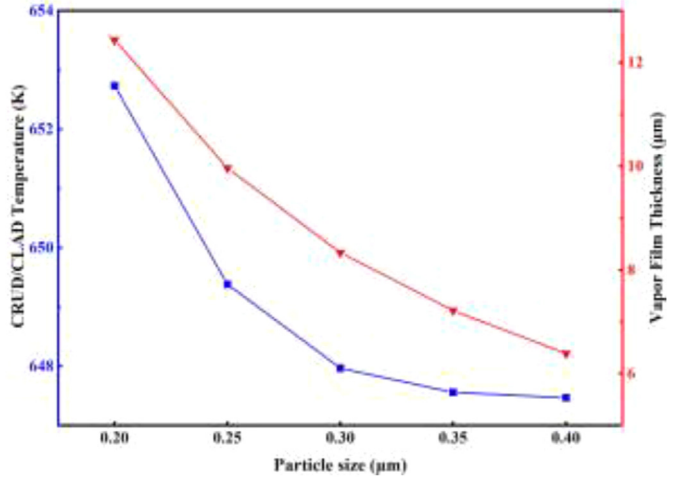

Fig. 9. Effect of CRUD particle size on CRUD/CLAD temperature and vapor film thickness.

The effect of the heat flux on the CRUD/CLAD temperature and the vapor film thickness is plotted in Fig. 10. With the increase of the heat flux, the CRUD/CLAD temperature monotonously increases, and the vapor film thickness increases rapidly first and then slowly when heat flux exceeds 0.7 MW/m^2. As the heat flux increases, the temperature increases, thus the vapor film thickness increases. With the further increase of the heat flux, the vapor heat thermal conductivity increases apparently, which can suppress the rise of the average temperature in the vapor-saturated region in a degree. Therefore, the increasing trend of the vapor film thickness with the heat flux decreases in the case of high heat flux.

3.3. Vapor film thickness correlation

After the sensitivity analysis of dependences of the vapor film thickness on the factors mentioned above, the multivariate linear regression is applied to assess the effect of the main factors (including the porosity, the chimney density, the CRUD thickness, the particle size and the heat flux) on the vapor film thickness. When each factor is concerned, the other factors are set to fixed values. The vapor film thickness is calculated with different factors. Through the multiple linear regression analysis of these factors, the correlation of the vapor thickness can be carried out as expressed in Eq. (32). Table 2 lists the details of the multivariate linear regression.

The probability of the F-test of multivariate linear regression is smaller than 0.05, indicating that the regression model is meaningful. In addition, the *P*-value of the partial regression coefficient by the t-test is smaller than 0.05, implying that each factor imposes a significant impact on the vapor film thickness. The multiple correlation coefficient R is equal to 0.98080. Therefore, the results of multiple correlation coefficient testing (F-test and t-test) indicate that the model meets the hypothesis testing of linearity and its matching effect is preferable.

In contrast to Eq. (1) reported by Ref. [14], the relationship between the vapor film thickness and its influential factors such as CRUD porosity, chimney density, CRUD thickness, particle size and

Table 2
The details of the multivariate linear regression.

I	1	2	3	4	5	Vapor film thickness (δ_v)
Simulated factors	Porosity (ε)	Chimney density (n_{ch})	CRUD thickness (δ)	Particle size (d_p)	Heat flux (q)	
Simulated range	0.40–0.70	1000–2000 mm^{-2}	10–30 μm	0.20–0.40 μm	5–10 × $10^5 W/m^2$	The calculated value range is 0.582–12.701 μm
Case step	0.05	200 mm^{-2}	5 μm	0.05 μm	1 × $10^5 W/m^2$	
Default value	0.40	2000 mm^{-2}	25 μm	0.25 μm	10 × 10^5 W/m^2	
Normalization (F_i)	$\frac{\varepsilon - 0.40}{0.70 - 0.40}$	$\frac{n_{ch} - 1000}{2000 - 1000}$	$\frac{10^6\delta - 10}{30 - 10}$	$\frac{d_p - 0.20}{0.40 - 0.20}$	$\frac{q - 5}{10 - 5}$	$\frac{\delta_v - 0.582}{12.701 - 0.582}$
Regression coefficient (R_i)	−0.89747	−0.19208	0.24163	0.46150	0.23123	___

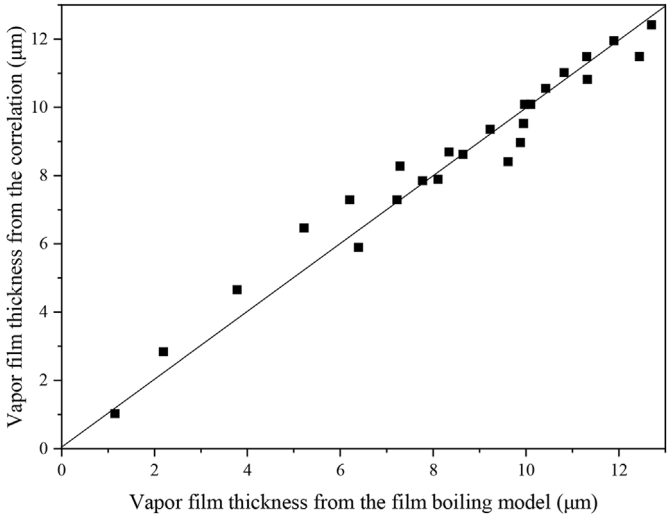

Fig. 11. Vapor film thickness calculated by the suggested correlation versus the data from the film boiling model.

heat flux can be reflected more intuitively in the obtained Eq. (32).

$$\frac{\delta_v - 0.582}{12.701 - 0.582} = \sum R_i F_i + 0.67007 + \begin{pmatrix} +0.11251 \\ -0.10325 \end{pmatrix} \quad (32)$$

where R_i is the regression coefficient of the different factors, and F_i represents the corresponding factor which are listed in Table 2. Eq. (32) can be transformed to Eq. (33) after the reduction.

$$\delta_v(\mu m) = -36.255\varepsilon - 2.3278 \times 10^{-3} n_{ch}\left(mm^2\right) + 1.4642\delta(\mu m) - 27.965 d_P(\mu m) + 0.56046 q\left(\frac{10^5 W}{m^2}\right) + 26.979 + \begin{pmatrix} +1.251 \\ -1.363 \end{pmatrix} \quad (33)$$

As shown in Fig. 11, the vapor film thickness obtained by the correlation (32) is well consistent with that calculated by the film boiling model coupled with Eq. (1). The correlation is valid to predict the vapor film thickness in CRUD under the condition of partial dry out, while the interaction of the disjointing force on the meniscus can be ignored. In our study, the range of various parameters are 0.40≤ ε ≤0.70, 1000≤ n_{ch} ≤2000 mm^{-2}, 15≤ δ ≤30 μm, 0.20 ≤d_p ≤ 0.40 μm, and 0.5 ≤ q ≤ 1.0 MW/m^2. In order to validate the extrapolated data by Eq. (33), the calculated vapor film thickness is 2.28 μm (i.e. the dry-out percentage is 3.8%), in the case of δ = 60 μm, ε = 0.50, n_{ch} = 3700 mm^{-2}, d_p = 0.40 μm and q = 0.95 MW/m^2, and this thickness is close to that predicted by the BOA codes(the dry-out percentage of 3.5%) [11].

The next step is introducing Eq. (33) into the film boiling model described in **section 2.1** to calculate the vapor film thickness. The distributions of the temperature, pressure and boric acid concentration in the CRUD recalculated by the film boiling model are presented in Fig. 12. The corresponding input parameters in Fig. 12 are listed in Table 3. In each graph of Fig. 12, the upper part corresponds to the liquid-saturated region and the bottom represents the vapor-saturated region, where the left boundary of each graph is the steam chimney wall and the right boundary is the symmetric line of a modeling unit of CRUD. The maximum temperature difference within the vapor-saturated region is 27 K, and 10 K in the liquid-saturated region as shown in Fig. 12(a). It indicates that the thermal resistance within the vapor-saturated region is significantly higher than that within the liquid-saturated region in CRUD. As shown in Fig. 12(b), the pressure difference along the chimney side is larger than that along the symmetric boundary both in the vapor-saturated region and in the liquid-saturated region. In Fig. 12(c) the boric acid concentration near the interface of the liquid and vapor region is significantly larger than that near the bulk coolant side, and the concentration factor of H_3BO_3 (ratio of maximum concentration to bulk concentration) in CRUD reaches about 30. This concentration factor is larger than that without consideration of the vapor film. In this case the CIPS risk increases to some extent. The temperature, pressure and boric acid concentration distributions in Fig. 12 are similar to the results obtained by the two-phase film boiling model coupled with the method of the vapor film thickness mentioned in **section 2**, and the latter results are not presented here for brevity.

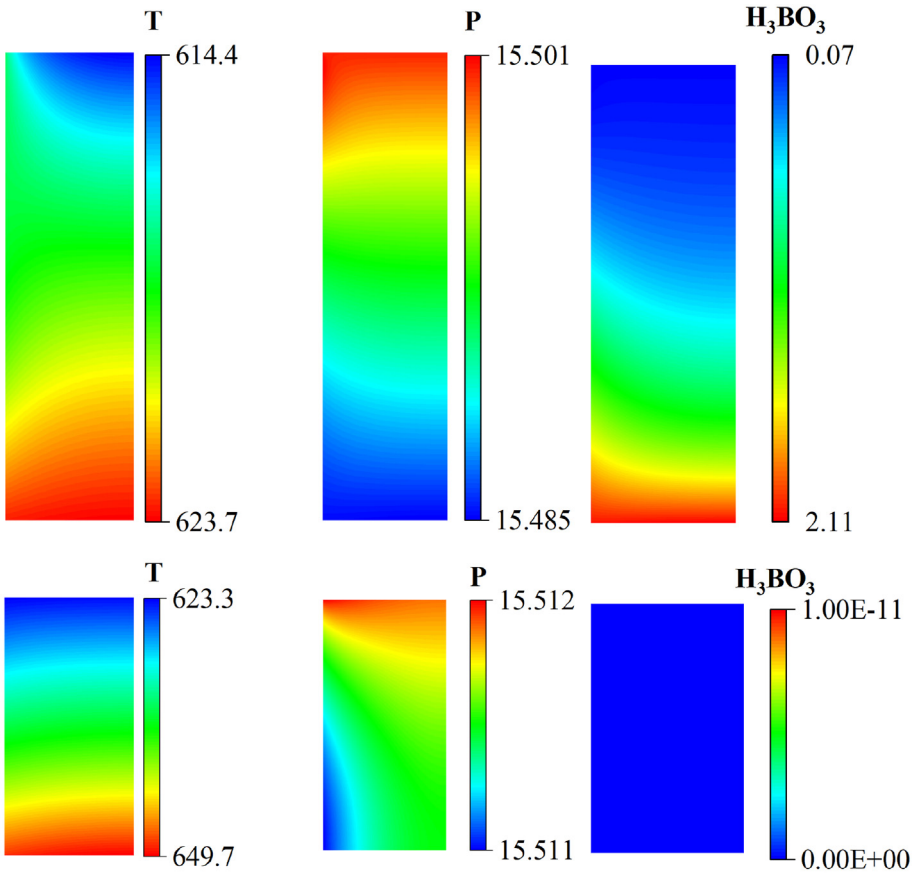

Fig. 12. Two-phase film boiling model results based on parameters from Table 3. Variable distributions in CRUD include: (a) temperature [K], (b) pressure [MPa] and (c) H_3BO_3 concentration [10^3 mol/m^3].

Table 3
Typical input values for simulating the film boiling.

Parameters	Value
Coolant Pressure(MPa)	15.5
Coolant Temperature(K)	600
Convective Heat Transfer Coefficient(W/m^2)	4.52×10^4
CRUD Porosity	0.60
CRUD Chimney Diameter(μm)	5
CRUD Maximum Pore Diameter(μm)	0.5
CRUD Minimum Pore Diameter(μm)	0.25
CRUD Thickness(μm)	25
Chimney Density(m^{-2})	2×10^9
Clad Surface Heat Flux(MW/m^2)	1.0

4. Conclusion

In this paper, a vapor thickness correlation in CRUD is proposed based on the sensitivity analysis and multivariate regression analysis, and the relationship between the vapor thickness and its influential factors such as CRUD porosity, CRUD chimney density, CRUD thickness, CRUD particle size and heat flux can be intuitively reflected. The temperature, pressure and boric acid concentration distributions in CRUD are calculated using the two-phase film boiling model coupled with the vapor thickness correlation. The cladding temperature and the CRUD dry-out percentage (which is reflected by the vapor film thickness) for different characteristics of the CRUD structure and different heat fluxes can be well predicted with the coupling of the vapor thickness correlation into the two-phase film boiling model. These results are helpful to reflect the heat transfer characteristics within CRUD in the case of partial dry-out.

Declaration of competing interest

The authors declare that they have no known competing financial interests or personal relationships that could have appeared to influence the work reported in this paper.

Acknowledgments

This work was financially supported by Sichuan Science and Technology Program (2021YJ0512).

References

[1] F. Carrette, M. Lafont, G. Chatainier, et al., Analysis and TEM examination of corrosion scales grown on Alloy 690 exposed to pressurized water at 325 °C, Surf. Interface Anal. 34 (1) (2002) 135–138.
[2] W.A. Byers, J. Deshon, Structure and chemistry of PWR crud, in: International Conference Water Chemistry in Nuclear Reactors Systems Conference, San Francisco USA, 2004, pp. 11–14.
[3] P. Athe, C. Jones, N. Dinh, Assessment of the predictive capability of VERA—CS for CASL challenge problems, Journal of Verification, Validation and Uncertainty Quantification 6 (2) (2021).
[4] N. Cinosi, I. Haq, M. Bluck, et al., The effective thermal conductivity of crud and heat transfer from crud-coated PWR fuel, Nucl. Eng. Des. 241 (3) (2011) 792–798.
[5] P. Cohen, Heat and mass transfer for boiling in porous deposits with chimneys 70 (138) (1974) 71–80.
[6] C. Pan, B.G. Jones, A.J. Machiels, Concentration levels of solutes in porous deposits with chimneys under wick boiling conditions, Nucl. Eng. Des. 99 (1985) 317–327.
[7] J. Henshaw, J.C. Mcgurk, H.E. Sims, et al., A model of chemistry and thermal hydraulics in PWR fuel crud deposits, J. Nucl. Mater. 353 (1–2) (2006) 1–11.

[8] I.U. Haq, Heat and Mass Transfer Analysis for Crud Coated PWR Fuel, Imperial College London, 2011.
[9] M. Short, D. Hussey, B. Kendrick, et al., Multiphysics modeling of porous CRUD deposits in nuclear reactors, J. Nucl. Mater. 443 (1–3) (2013) 579–587.
[10] B.G. Park, S. Seo, S.J. Kim, et al., Meso-scale multi-physics full coupling within porous CRUD deposits on nuclear fuel, J. Nucl. Mater. 512 (2018) 100–117.
[11] G. Wang, Improved Crud Heat Transfer Model for Dryout on Fuel Pin Surfaces at Pwr Operating Conditions, The Pennsylvania State University, 2009.
[12] M. Jin, M. Short, Multiphysics modeling of two-phase film boiling within porous corrosion deposits, J. Comput. Phys. 316 (2016) 504–518.
[13] J. Collier, J. Thome, Convective Boiling and Condensation, third ed., Oxford University Press, 1994.
[14] D.Y. Yeo, H.C. No, Modeling heat transfer through corrosion product deposits on fuel rods in pressurized water reactors, Nucl. Eng. Des. 342 (2019) 308–319.
[15] S. Dickinson, J. Henshaw, J.C. McGurk, et al., Modeling PWR Fuel Corrosion Product Deposition and Growth Processes, EPRI, Palo Alto, CA, 2004, p. 1009734.
[16] J. Deshon, PWR Axial Offset Anomaly (AOA) Guidelines, Revision 1, EPRI, Palo Alto, CA, 2004, 1008102.
[17] Ying Shi, Jinsheng Xiao, Shuhai Quan, Mu Pan, Runzhang Yuan, Fractal model for prediction of effective thermal conductivity of gas diffusion layer in proton exchange membrane fuel cell, J. Power Sources 185 (1) (2008) 241–247.
[18] D.Y. Yeo, H.C. No, Modeling film boiling within chimney-structured porous media and heat pipes, Int. J. Heat Mass Tran. 124 (2018) 576–585.
[19] W. Woodside, J.H. Messmer, Thermal conductivity of porous media. II. Consolidated rocks, J. Appl. Phys. 32 (9) (1961) 1699.
[20] P.J. Gierszewski, B.B. Mikic, N.E. Todreas, Property Correlations for Lithium, Sodium, Helium, Flibe and Water in Fusion Reactor Applications, Massachusetts Institute of Technology, Plasma Fusion Center, 1980.
[21] J. Deshon, Simulated Fuel Crud Thermal Conductivity Measurements under Pressurized Water Reactor Conditions, EPRI, 2011. Technical Report 1022896.
[22] J.L. Uhle, Boiling Heat Transfer Characteristics of Steam Generator U-Tube Fouling, Massachusetts Institute of Technology, 1997.
[23] R. Salko Jr., T.L. Lange, E. Tatli, et al., Development of a Crud Induced Localized Corrosion Analysis Capability in VERA, Oak Ridge National Lab.(ORNL), Oak Ridge, TN (United States), 2020.